



Contents lists available at *Dergipark*

Journal of Scientific Reports-A

journal homepage: <https://dergipark.org.tr/pub/jsr-a>



E-ISSN: 2687-6167

Number 58, September 2024

RESEARCH ARTICLE

Receive Date: 04.04.2024

Accepted Date: 17.05.2024

Mathematical modelling and performance analysis of an AEM electrolyzer

Salih Obut^{a,*}

^a*Yildiz Technical University, Department of Mechatronics Engineering, İstanbul 34349, Türkiye, sobut@yildiz.edu.tr
ORCID: 0000-0002-9833-8151*

Abstract

In this study, an analytical model including electrochemical reactions and mass transfer in an anion-exchange membrane electrolyzer (AEMEL) has been developed by considering water sorption/desorption in electrodes. The model developed was used to investigate the performance of the AEMEL in terms of efficiency, transport phenomena and operating parameters. The numerical results revealed that the voltage losses in the AEMEL are mainly due to activation losses. The effects of important parameters such as membrane thickness, operating pressure on cell performance, and species transport were also investigated. The results also revealed that the AEMEL performance improves with decreasing membrane thickness, but the membrane thickness should be considered together with hydrogen permeability and differential operating pressure to operate the electrolyzer safely.

© 2023 DPU All rights reserved.

Keywords: Anion exchange membrane; transport phenomena; water electrolyzer; membrane thickness; mathematical modelling.

1. Introduction

Hydrogen is defined as the clean energy carrier of the future. Hydrogen presents several benefits over fossil fuels as an energy carrier; one of them is the hydrogen energy content (120 MJ/kg), which is higher than most fuels (e.g.

* Corresponding author. Tel.: +90-535-884-2154; fax: +90-212-383-2975.

E-mail address: sobut@yildiz.edu.tr

<http://dx.doi.org/10.1016/j.cviu.2017.00.000>

natural gas 48.7 MJ/kg). In addition, the use of hydrogen in industry has the potential to eliminate the greenhouse gas emission problems caused by the use of fossil fuels.

Hydrogen can be produced from fossil-based sources as well as water by various methods such as thermal, photocatalytic etc. processes. Nowadays, electrolysis of water with renewable energy sources is seen as a sustainable and cost-effective solution for green hydrogen production and intensive research and development activities are carried out on electrolyzers [1,2].

There are three important low-temperature electrolyzer technologies in hydrogen production; alkaline electrolyzer (AEL), proton-exchange membrane electrolyzer (PEMEL) and anion-exchange membrane electrolyzer (AEMEL). AELs are seen as the most mature technology. Although they are economical in initial investment cost, they require high electrolyte concentrations, and purification and pressurization of hydrogen at the electrolyzer exit. Compared to AEL technology, PEMELs have the advantage of high hydrogen outlet pressure and high purity due to the use of membrane as the anode-cathode separator material in their structures. However, materials, such as Pt, Pd, and Ir, used in PEMELs significantly increase the initial investment costs of these electrolyzers. On the other hand, AEMELs are seen as an alternative that combines the advantages of both alkaline and PEMELs. AEMEL, like PEMEL, have a membrane as separator in their structure and therefore can provide hydrogen of high purity and pressure at the output. Additionally, unlike AEL, they can be operated with a very low concentration of electrolyte solution, that reduces corrosion, and with lower priced catalysts based on Cu, Ni, Co, and Fe. Therefore, due to these advantages among electrolyzer technologies, intensive research and development studies are carried out on AEM electrolyzer in the last decades.

Mathematical modelling is an important tool used in improving the performance and examining the behavior of complex physicochemical processes. Design and optimization of AEMELs, which are still at low technology readiness level (TRL), through mathematical modeling are gaining importance. There are limited number of publications in the literature on modelling AEMELs [3-8]. An et al. [3] examined the effects of liquid saturation, exchange current density and membrane thickness on the performance of an AEMEL. Nafchi et al. [4] investigated different parameters such as cell temperature and cathode pressure levels of AEM. Vidales et al. [5] developed a model that considers mass transfer and electrochemistry together to evaluate the effects of electrolyzer parameters. The model was then validated and effect of the operating parameters of electrolyzer such as electrolyte concentration, temperature, and operating pressure were evaluated. Liu et al. [6] presented a two-phase one-dimensional AEMEL model that is extended from their previous work. The results indicated that electrolyte concentration has more impact on oxygen evolution reaction (OER) kinetics than AEM conductivity. Stainslaw et al. [7] analyzed the effect of electrolyte composition and they found that the conductivity of membrane has insignificant impact on the electrolyzer performance. Kim et al. [8] presented a deterministic model and a feasibility analysis of a 10 MW AEMEL system. The results revealed that the levelised cost of hydrogen (LCOH) of AEMEL would be comparable to that of PEMEL when the lifetime of AEMEL is brought to the same level as PEMEL.

In the present study, an isothermal analytical model is proposed to assess the performance of an AEMEL. The developed model considers transport within gas phase, liquid phase and ionomer/membrane phase together with electrochemical effects. In contrast to the lumped models in the literature, the model was developed to include the ionomer phase sorption/desorption rates explicitly. In this way, it is possible to model the decrease of membrane water content on the cathode electrode due to increasing current density, i.e. electro-osmotic drag effect, and thus the loss of performance of AEMEL. The model is then used to predict current-voltage polarization, efficiency and product stream compositions of the electrolyzer. The governing model equations were solved in the MATLAB environment and the model was validated with literature data. The performance of the electrolyzer was analyzed for different membrane thicknesses and different operating pressures through parametric analysis.

2. Mathematical model

The AEM electrolyzer model can be obtained by combining the mass transport and the electrochemical model equations. The electrochemical model equations are written for prediction of the operating voltage of the cell, considering voltage losses in the cell, such as activation losses, ohmic losses, etc. The mass transport equations are used to predict the transport of water across the membrane, the consumption production rates of the components at the anode and at the layer, and the transport of OH⁻ and water molecules across the membrane. By solving set of these coupled equations, the cell voltage, efficiency and product gas stream compositions can be predicted at different current densities.

A typical AEM electrolyzer cell has a membrane, anode and cathode electrodes (catalyst and diffusion layers) and bipolar plates on which flow channels are engraved. The electrolyte solution, i.e. typically aqueous KOH solution, is fed to the electrolyzer anode side while no solution is delivered to the electrolyzer cathode side. The water in the electrolyte solution in anode is transferred to the other side of the membrane to meet the water demand of the hydrogen evolution reaction (HER). The water transferred to the cathode side is reduced to hydroxide and hydrogen by the HER in the electrode (Equation 1). The resulting hydroxide ions pass to the anode side through the AEM and are oxidized in the anode electrode (Equation 2) to release oxygen (Fig. 1). Oxygen and hydrogen formed within the two sides of the electrolyzer leave the electrolyzer cell through the flow channels in the bipolar plates. Fluid flow in the anode flow channels is multiphase (i.e. mostly oxygen + KOH solution), whereas in the cathode flow channels, which are not supplied with KOH solution, only gas-phase flow is present (dry operation).

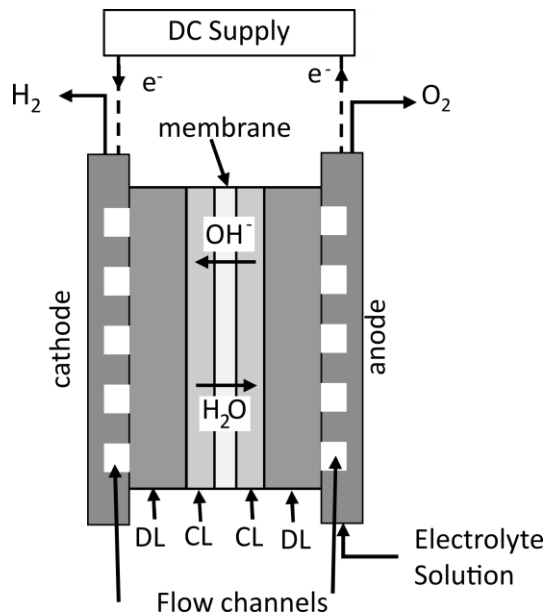
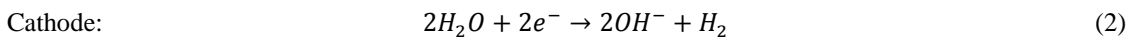
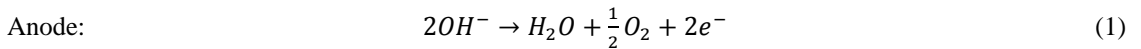


Fig. 1. Structure of a single cell AEMEL.

2.1. Electrochemical equations

The electrochemical behavior of an electrolyzer can be described by the following current-voltage (I-V) model, including the most important voltage losses that determine the cell voltage, E_{cell}

$$E_{cell} = E_{rev} + \eta_{act} + \eta_{ohm} + \eta_{conc} \quad (3)$$

where E_{rev} is the reversible cell voltage, η_{act} is the activation losses or overpotential, η_{ohm} is the ohmic losses or overpotential, and η_{conc} is the mass transfer losses or overpotential. The other overpotentials such as bubble overpotential etc. were neglected.

The reversible cell voltage, $E_{rev}(T, P)$, of an electrolyzer system in which hydrogen and oxygen evolution reactions present is governed by the Nernst equation

$$E_{rev}(T, P) = E_{rev}^0(T) + \frac{RT}{2F} \ln \left(\frac{\prod p_p}{\prod p_r} \right) \quad (4)$$

where $E_{rev}^0(T)$ is the reversible cell voltage (V), R is the ideal gas constant, F is Faraday's constant, p_r and p_p are reactants and products partial pressures. Reversible cell potential, $E_{rev}^0(T)$ in voltage, can be calculated by using [9]

$$E_{rev}^0(T) = 1.481 - 0.000846T(K) \quad (5)$$

for $H_2O_{(l)}$ at 25°C. The reversible cell voltage, $E_{rev}(T, P)$ in V, is given as a function of pressure and temperature [9]

$$E_{rev}(T, P) = 1.481 - 0.000846T(K) + 0.0000431T(K) \ln \left(\frac{p_{H_2} p_{O_2}^{0.5}}{p_{H_2O}} \right) \quad (6)$$

where p_{H_2} , p_{O_2} , and p_{H_2O} are corresponding species partial pressures, respectively. The activation overpotential, η_{act} , is the potential required to overcome the activation energies of the HER and OER occurred at cathode and anode of an electrolyzer. The activation overpotential can be explicitly calculated as follows

$$\eta_{act} = \eta_{act,an} + \eta_{act,ca} = \frac{RT}{\alpha_{an}F} \operatorname{arcsinh} \left(\frac{i}{2j_{o,an}} \right) + \frac{RT}{\alpha_{ca}F} \operatorname{arcsinh} \left(\frac{i}{2j_{o,ca}} \right) \quad (7)$$

where α represents the charge coefficient and j_o represents the apparent exchange current density value which is function of the physical properties of electrodes, i.e. roughness, and the exchange current density at reference temperature and operating temperature [10].

The ohmic overpotential, η_{ohm} , is arising due to the current-carrying components resistance to electron transport and ion-conducting media resistance to ion transport. The ohmic overpotential is given by Ohm's law

$$\eta_{ohm} = R_{cell}I = (R_{el} + R_{ion})I \quad (8)$$

where R_{cell} is the ohmic resistance of the cell and I is the current. In Equation 8, R_{el} is the resistance of electron conducting media, i.e. bipolar plates and electrodes, and R_{ion} is the total resistance of ion conducting media, i.e. ionomer phase and electrolyte solution in electrodes and membrane, within cell. In this study, because electron

transport resistances are expected to be lower than that of ion transport resistances, for simplicity, only the resistance of ion conducting media is considered

$$R_{ion} = R_{mem} + R_{ion,an} + R_{ion,ca} \quad (9)$$

where R_{mem} , $R_{ion,an}$, and $R_{ion,ca}$ corresponds ionic resistances of membrane, anode catalyst layer (ACL) and cathode catalyst layer (CCL), respectively, i.e. ionomer and electrolyte resistances for anode and only ionomer resistance in cathode. Resistance of membrane is given by

$$R_{mem} = \frac{\delta_{mem}}{\sigma_{mem}A} \quad (10)$$

where δ_{mem} is the membrane thickness, σ_{mem} is the membrane conductivity and A represents cell active area. Similarly, catalyst layer (CL) ionic resistances are calculated by

$$R_{ion,an} = \left[\frac{\delta_{CL}}{\sigma_{ion}^{eff}A} + \frac{\delta_{CL}}{\sigma_{KOH}^{eff}A} \right]^{-1} \quad (11)$$

$$R_{ion,ca} = \frac{\delta_{CL}}{\sigma_{ion}^{eff}A} \quad (12)$$

where δ_{CL} is the CL thickness, σ_{ion}^{eff} and σ_{KOH}^{eff} are effective ionomer and electrolyte solution conductivities, respectively, that are corrected by Bruggeman relation [11]. In anode catalyst layer, it is assumed that resistance of ionomer phase and KOH solution was considered as parallel resistances.

The mass transfer overpotential, η_{conc} , represents the losses due to diffusion processes and sometimes called as concentration losses or overpotential. In this study, it is assumed that concentration overpotential is negligible; therefore, this term is neglected in the present model.

2.2. Mass transport equations

The mass transfer in the AEM electrolyzer cell was obtained by writing the mass balances of each species for each phase in anode, cathode, and membrane. On the anode side, mass balances of H_2 , O_2 and H_2O in the gas phase and mass balances of KOH and water in the liquid phase were considered. On the cathode side, mass balances were established for H_2 and H_2O in the gas stream. In order to resolve H_2O transport between two sides of the electrolyzer cell, mass balance of dissolved water in ionomer/membrane was established for ACL and CCL and membrane. Furthermore, the mass balances were linked to the electrochemical model by means of the production and consumption rate equations of hydrogen, oxygen and water in the ACL and CCL.

The molar generation rate and consumption rate of H_2 , O_2 and H_2O can be written according to Faraday's law. For the anode side where O_2 and H_2O generated

$$N_{O_2,an}^{gen} = \frac{I}{4F} \quad (12)$$

$$N_{H_2O,an}^{gen} = \frac{I}{2F} \quad (13)$$

and for cathode side where H_2 generated and H_2O consumed

$$N_{H_2,ca}^{gen} = \frac{I}{2F} \quad (14)$$

$$N_{H_2O,ca}^{cons} = \frac{I}{F} \quad (15)$$

The mass balance of species in anode side can be written for gas and liquid phases separately. For gas phase, hydrogen balance is

$$N_{H_2,an}^{in} - N_{H_2,an}^{out} + N_{H_2,mem}^{perm} = 0 \quad (16)$$

where superscripts *in* and *out* represents inlet and outlet flow rates. Hydrogen crossover through the membrane, $N_{H_2,mem}^{perm}$, is given by

$$N_{H_2,mem}^{perm} = k_{H_2} \frac{A}{\delta_{mem}} (P_{ca} - P_{an}) \quad (17)$$

where k_{H_2} is the permeability of hydrogen, P_{ca} and P_{an} are cathode and anode pressures. For gas phase, O_2 balance is

$$N_{O_2,an}^{in} - N_{O_2,an}^{out} + N_{O_2,an}^{gen} = 0 \quad (18)$$

where O_2 generation is given by Equation 12. Similarly, for the gas phase H_2O mass balance

$$N_{H_2O,an}^{in} - N_{H_2O,an}^{out} + N_{H_2O,an}^{phase} = 0 \quad (19)$$

where $N_{H_2O,an}^{phase}$ account for water transfer from liquid phase to gas phase in anode side. In this model, because aqueous KOH solution is fed to the anode side, it is assumed that the anode outlet gas is saturated with water until it leaves the cell. With the aid of this assumption, the mass transfer rate from liquid phase to gas phase, $N_{H_2O,an}^{phase}$, was calculated during the simultaneous solution of the anode and cathode mass balances. For anode side liquid phase, KOH and water balances are written

$$N_{KOH,an}^{in} - N_{KOH,an}^{out} = 0 \quad (20)$$

$$N_{H_2O,l,an}^{in} - N_{H_2O,l,an}^{out} - N_{H_2O,an}^{phase} - N_{H_2O,an}^{sorp} = 0 \quad (21)$$

where $N_{H_2O,an}^{sorp}$ represent water transfer from liquid phase to ionomer phase within ACL. Because aqueous KOH solution was fed to the anode side, the ionomer in the ACL was considered fully saturated. Again, similar to the liquid-gas water transfer rate in anode, the sorption rate of water will be calculated by solving two side mass balances above simultaneously.

The mass balance for cathode side of the cell can be written. For gas phase, H_2 and H_2O balances are given below

$$N_{H_2,ca}^{in} - N_{H_2,ca}^{out} + N_{H_2,ca}^{gen} - N_{H_2,mem}^{perm} = 0 \quad (22)$$

$$N_{H_2O,ca}^{in} - N_{H_2O,ca}^{out} + N_{H_2O,ca}^{desorp} = 0 \quad (23)$$

where $N_{H_2O,ca}^{desorp}$ is the desorption rate of dissolved water from ionomer phase to gas phase which is given by

$$N_{H_2O,ca}^{desorp} = \gamma_{dw} (C_{dw,ca} - C_{dw,ca}^{eq}) V_{CL,ca} \quad (24)$$

Rate constant for membrane/ionomer desorption/sorption process, γ_{dw} , is taken as 100 s^{-1} [12,13]. The actual and the equilibrium dissolved water concentrations are denoted by $C_{dw,ca}$ and $C_{dw,ca}^{eq}$, respectively. Catalyst layer volume, $V_{CL,ca}$, is simply product of active area and cathode catalyst layer thickness. Equilibrium dissolved water concentration can be calculated by [14]

$$C_{dw}^{eq} = p_m \lambda^{eq} \quad (25)$$

where p_m is the product of membrane dry density, ρ_{dry} , and ion exchange capacity (IEC) and λ^{eq} is the equilibrium water content, that is defined as the number of water molecules per positively charged (cationic) functional groups (FG) within membrane [15].

The dissolved water transport through membrane/ionomer can be written in terms of diffusion, electro-osmotic drag (EOD) effect, and hydraulic pressure (HP) effect. Thus, net rate of dissolved water transport from ACL to CCL

$$N_{H_2O,mem}^{net} = N_{H_2O,mem}^{diff} - N_{H_2O,mem}^{eod} - N_{H_2O,mem}^{perm} \quad (26)$$

where $N_{H_2O,mem}^{net}$ is the rate of net molar transport of dissolved water, $N_{H_2O,mem}^{diff}$ is the molar transport rate of dissolved water by diffusion from ACL to CCL, $N_{H_2O,mem}^{eod}$ is the rate of molar transport H_2O from CCL to ACL due to EOD and $N_{H_2O,mem}^{perm}$ is the molar transport rate of dissolved water from the CCL to the ACL due to the pressure differential.

The diffusion rate of water is calculated by Fick's law in the CCL assuming fully hydrated conditions for membrane

$$N_{H_2O,mem}^{diff} = N_{H_2O,ca}^{diff} = D_w A (C_{dw,mem}^{eq} - C_{dw,ca}) / \delta_{CL,ca}^{eff} \quad (27)$$

where D_w is the water diffusion coefficient of in the ionomer phase, $\delta_{CL,ca}^{eff}$ is the effective diffusion path within CCL, which is taken to be half of the thickness of the cathode catalyst layer. $C_{dw,mem}^{eq}$ is the equilibrium dissolved water concentration within wet membrane and $C_{dw,ca}$ is the dissolved water concentration in the ionomer phase of CCL.

The H_2O transport due to EOD is related to the flux of hydroxides migrating from the CCL to ACL through the AEM and can be expressed as

$$N_{H_2O,mem}^{eod} = n_d \frac{i}{F} \quad (27)$$

where n_d is the EOD coefficient (mol H_2O / mol OH^-). Electro-osmotic drag coefficient is function of H_2O content of ionomer/membrane and for the simplicity it is taken as 5 mol H_2O / mol OH^- [16].

The H_2O transport rate from the CCL to the ACL through the membrane can be calculated using Darcy's law

$$N_{H_2O,mem}^{perm} = K_D \frac{A}{\delta_{mem}} (P_c - P_a) \frac{\rho_{H_2O}}{\mu_{H_2O}} \quad (28)$$

where K_D is the H_2O permeability of membrane.

Dissolved water balance for anode side can be written in terms of net molar transport rate of dissolved water as

$$N_{H_2O,an}^{sorp} + N_{H_2O,an}^{gen} - N_{H_2O,mem}^{net} = 0 \quad (29)$$

where $N_{H_2O,an}^{gen}$ is the generation of water by Equation 1 in anode. Similarly, for cathode dissolved water balance can be written

$$N_{H_2O,mem}^{net} - N_{H_2O,ca}^{cons} - N_{H_2O,ca}^{desorp} = 0 \quad (30)$$

where $N_{H_2O,ca}^{cons}$ is the consumption of water by Equation 2 in cathode.

2.3. Solution methodology

Mass transport model and electrochemical model given in the previous section were solved by MATLAB. The baseline model and operating parameters are given in Table 1 and Table 2, respectively. In the next section, the validation of model and series of parametric analysis regarding the AEMEL performance are presented.

Table 1. The model parameters.

Parameter	Value	Unit	Reference
R	8.314	$J \text{ mol}^{-1} \text{ K}^{-1}$	
F	96,485.3	$A \text{ s mol}^{-1}$	
Density of water, ρ_{H_2O}	998.04	$kg \text{ m}^{-3}$	
Water viscosity, μ_{H_2O}	5.465×10^{-4}	$kg \text{ m}^{-1} \text{ s}^{-1}$	
Membrane Darcy water permeability, K_D	1×10^{-20}	m^2	[17], [18]
Vapor equilibrated membrane water content, λ	Eqns. 27-29 in [16]	$\frac{\text{mol } H_2O}{\text{mol } FG}$	[16]
Wet membrane water content, λ^{eq}	18.5	$\frac{\text{mol } H_2O}{\text{mol } FG}$	[16]
Apparent OER exchg. current density, $j_{0,an}$	1.9	mA cm^{-2}	[19]
Apparent HER exchg. current density, $j_{0,ca}$	5.6×10^{-2}	mA cm^{-2}	[20]
Diffusion coefficient of water, D_w	Eqns. 30-31 in [16]	$\text{m}^2 \text{ s}^{-1}$	[16]
Electro-osmotic drag coefficient, n_d	5	$\frac{\text{mol } H_2O}{\text{mol } OH^-}$	[16]
Thickness of membrane, δ_{mem}	28	μm	[16]
Membrane IEC	1.8	meq g^{-1}	[16]
ACL thickness, $\delta_{CL,an}$	30	μm	Assumption
CCL thickness, $\delta_{CL,ca}$	15	μm	Assumption
ACL porosity, $\epsilon_{CL,an}$	0.2		Assumption
CCL porosity, $\epsilon_{CL,ca}$	0.1		Assumption
Ionomer volume fraction of ACL, $\epsilon_{ion,CL,an}$	0.6		Assumption
Ionomer volume fraction of CCL, $\epsilon_{ion,CL,ca}$	0.6		Assumption
Hydrogen permeability, k_{H_2}	5.6×10^{-17}	$\text{mol s}^{-1} \text{ cm}^{-1} \text{ Pa}^{-1}$	[21]

Conductivity of KOH solution	Eqn. 2 in [22]	S cm^{-1}	[22]
Cell active area, A	25	cm^2	

Table 2. AEMEL operating parameters.

Parameter	Value	Unit
Temperature, T	50	$^{\circ}\text{C}$
Anode pressure, P_a	1	bar
Cathode pressure, P_c	1	bar
Concentration of KOH solution	10	mM
Feed flow rate of KOH solution	20	ml min^{-1}

3. Results and discussions

In this part, firstly, the validation of the model using literature data is presented. Then, the effects of parameters such as membrane thickness and operating pressure on the cell performance and species transport are presented.

3.1. Model validation

Before performing parametric analysis with the developed model, the predictive ability of the model was evaluated by comparing the polarization curve generated by the model with the experimental polarization curve of the dry cathode AEM electrolyzer in [23] under the same conditions. Fig. 2 shows that the polarization curve predicted by the model is in good agreement with the experimental data. In the next part, numerical results for the effects of operating pressure and of membrane thickness and are presented, respectively.

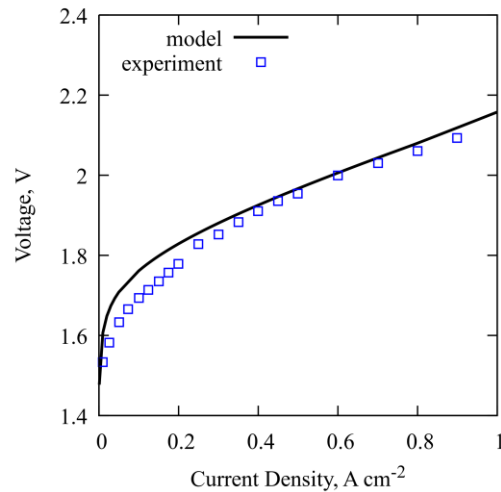


Fig. 2. Developed model polarization curve and experimental data [23].

3.2. Effect of membrane thickness

In AEMELs, membrane thickness has an impact on the ionic resistance of the cell, water transport, and hydrogen permeability through the membrane. While reducing the membrane thickness, it improves performance by reducing

the ionic resistance and increasing the amount of H_2O transported from the ACL to the CCL. It can also increase hydrogen transfer from the cathode side to the anode side for cells operating with a pressure difference between the cathode and anode. This could pose a safety issue and reduce Faraday efficiency. Therefore, cell polarization curves were estimated by using the validated model for two different cases where the membrane thickness was halved and doubled compared to the initial case. According to Fig. 3, the cell performance improves inversely proportional to the membrane thickness and the increase in performance with decreasing membrane thickness has been observed in many modeling [3, 5] and experimental studies [24-26] in the literature. Improvement is mainly due to ionic resistance, i.e. ohmic overpotential and this is evident from the increase in the slope of the polarization curve at high current densities. The effect of thickness of membrane was also studied for cells operating with a pressure difference between the cathode side and anode side. In this case, electrolyzer performance was predicted for 30 bar pressure difference ($\Delta P = P_c - P_a = 30 \text{ bar}$) between cathode and anode (Fig. 4). The results in Fig. 4(a) show that both Faraday efficiency and DC efficiency of the cell (based on higher heating value, HHV, of H_2) decreases with decreasing membrane thickness as a result of increasing hydrogen crossover (Fig. 4(b)). At 0.5 mA cm^{-2} current density and with $28 \mu\text{m}$ membrane thickness, anode product gas may contain 3.9% vol. hydrogen (Fig. 4(b)) which is very close to lower explosive limit (LEL) limit [27], 4% in 1 bar. For atmospheric operation, the amount of H_2 in O_2 was experimentally found to be about 0.14% vol. [23], however, H_2 permeation will be much higher for a pressure difference of 30 bar. Considering that the H_2 flux increases in direct proportion to the pressure difference, H_2 in O_2 is likely to be around 4% for 30 bar pressure difference operation, which agrees with the 3.9% value obtained from this modeling study. In order to reach hydrogen content in anode gas below LEL limit, current density values greater than approximately 1 A/cm^2 is required. For the safe operation of the AEM electrolyzer with a reasonable threshold, i.e. 2% below LEL limit, nearly 1 A cm^{-2} is required for membrane thickness of $28 \mu\text{m}$.

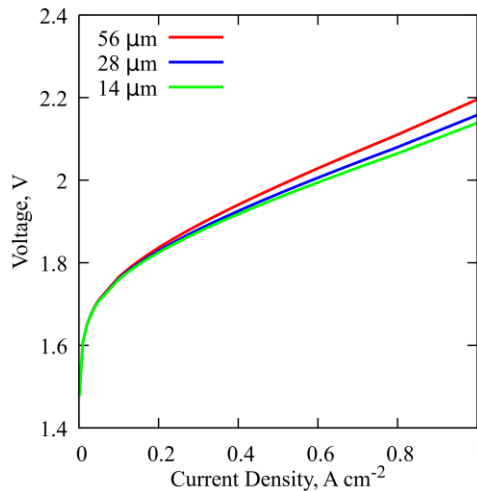


Fig. 3. Polarization curves for different membrane thicknesses.

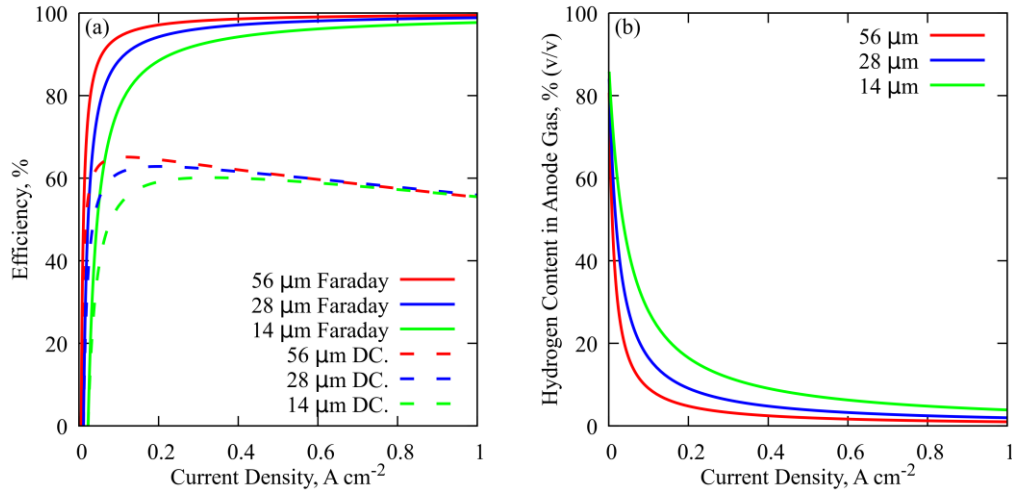


Fig. 4. (a) Faraday efficiency (continuous line) and DC efficiency (dashed line), (b) hydrogen mole percentages for different membrane thicknesses at 30 bar pressure difference between cathode side and anode side.

3.3. Effect of operating pressure

Another operating parameter that affects the performance of an AEM electrolyzer operating in dry cathode mode is the cathode and anode side pressure difference at the same membrane thickness. The cathode side pressure of AEMELs is tried to be kept high to prevent the need for additional pressurization of the produced hydrogen. However, this situation has negative effects. First, as it can be seen by the Nernst equation, the electrolyzer cell operating voltage increases as the effect of the increasing pressure difference. Additionally, increasing differential pressure increases the hydrogen cross-over from the cathode to the anode, reducing the Faraday efficiency. Finally, due to the increasing cathode-anode differential pressure, water transfer increases from cathode side to the anode side, and this can reduce the cathode side ionomer water content along with the decreasing relative humidity especially at high current densities. This increases the cell resistance to ion transport and causes performance decrease.

Effect of cathode-anode pressure difference on AEM electrolyzer performance is shown in Fig. 5(a). Because a high operating pressure directly increases the open circuit voltage, the cell polarization curve tends to increase at high pressure differences. However, while this effect is evident up to 15 bar pressure difference from atmospheric operation, it is not evident between 15 and 30 bar pressure difference. In their study, Nafchi et al. [4] also found that the cell operating voltage increased with increasing cathode side pressure and this increase was much less pronounced after 10 bar cathode pressure. Besides the effects of pressure increase, the increasing cathode-anode pressure difference increases the amount of water hydraulically passing from the cathode side to the anode side, thereby reducing the H_2O content of the cathode side ionomer phase and thus increasing the ohmic polarization. Additionally, the humidity of the cathode product gas will decrease as an effect of decreasing net water transport to the CCL. Water content of the CCL ionomer phase is shown in Fig. 5(b). As can be seen, with increasing cathode-anode pressure difference, the water content and therefore the conductivity of the cathode ionomer phase decreases. This can be understood from the fact that the polarization curves in Fig. 5(a) slope upward in the high current density region.

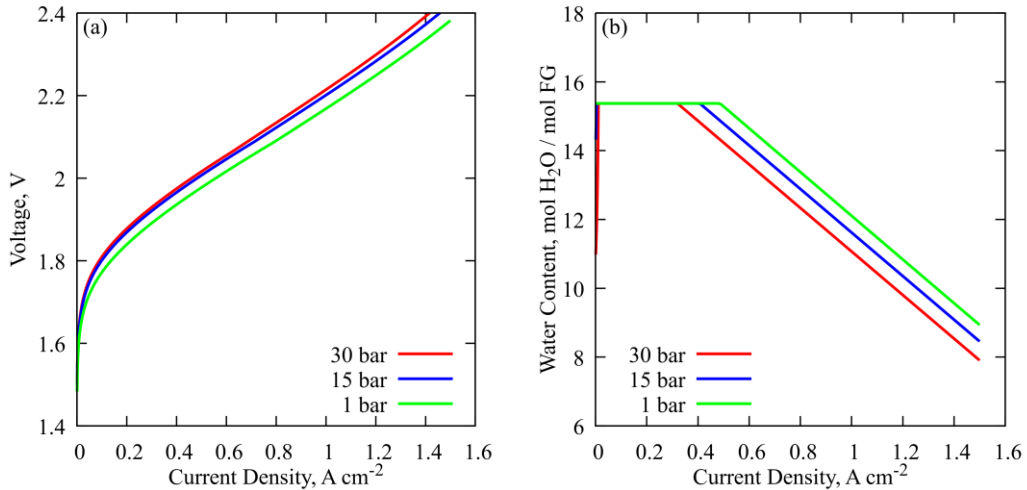


Fig. 5. (a) Polarization curves, (b) cathode side ionomer phase water contents for various pressure differential between cathode and anode.

4. Conclusions

In this study, an analytical model was developed to predict the performance of an AEMEL fed with aqueous KOH solution to anode. The developed model was validated with literature data and then analyses were carried out with the help of the model for two important parameters that determine the AEM electrolyzer performance. Accordingly, as the membrane thickness decreases, both the AEMEL cell voltage and the Faraday and DC efficiency of the cell decreases. Higher operating pressure of cathode side is one of the advantages of AEMEL technology, however, at high pressure differences between the cathode and anode side, such as 30 bar, a gas mixture with H₂ content above 4% vol. may form at the anode outlet, which poses a safety risk. Therefore, the most suitable membrane thickness should be selected according to the operating conditions by considering the compromise between cell voltage, efficiency and cell operating safety. On the other hand, when the pressure is increased at constant membrane thickness, it is found that the AEMEL polarization curves tend to increase upward more at high current densities above 1 A cm⁻² as a result of decreased cathode side membrane water content. Thus, especially for large active area electrolyzer stacks drying of cathode side should be properly handled and this requires higher dimensional model of AEMEL to see the local drying effects. In order to better understand local effects at the cell level, studies are ongoing to adapt the model to two-dimensions and eventually to three-dimensions.

Author contribution

The writing of the manuscript and all analyses were performed by Salih Obut.

Acknowledgements

The author would like to thank Prof.Dr. Serdar S. Çelebi for the valuable discussions on the results of the study.

References

- [1] IRENA, "World Energy Transitions Outlook 2023: 1.5°C Pathway," Abu Dhabi, 2023. [Online]. Available: <https://www.irena.org/Publications/2023/Jun/World-Energy-Transitions-Outlook-2023> Accessed: Feb. 7, 2024.
- [2] IEA, "Global Hydrogen Review 2023," Paris, 2023. [Online]. Available: <https://www.iea.org/reports/global-hydrogen-review-2023>. Accessed: Feb. 7, 2024.
- [3] L. An, T. S. Zhao, Z. H. Chai, P. Tan, and L. Zeng, "Mathematical modeling of an anion-exchange membrane water electrolyzer for hydrogen production," *Int. J. Hydrogen Energy*, vol. 39, no. 35, pp. 19869-19876, 2014.
- [4] F. M. Nafchi, E. Afshari, and E. Baniasadi, "Anion exchange membrane water electrolysis: Numerical modeling and electrochemical performance analysis," *Int. J. Hydrogen Energy*, vol. 52, pp. 306-321, 2024.
- [5] A. G. Vidales, N. C. Millan, and C. Bock, "Modeling of anion exchange membrane water electrolyzers: The influence of operating parameters," *Chem. Eng. Res. Des.*, vol. 194, pp. 636-648, 2023.
- [6] J. Liu, Z. Kang, D. Li, M. Pak, S. Alia, et al., "Elucidating the role of hydroxide electrolyte on anion-exchange-membrane water electrolyzer performance," *J. Electrochem. Soc.*, vol. 168, no. 5, p. 054522, 2021.
- [7] L. N. Stanislaw, M. R. Gerhardt, and A. Z. Weber, "Modeling electrolyte composition effects on anion-exchange-membrane water electrolyzer performance," *ECS Trans.*, vol. 92, no. 8, p. 767, 2019.
- [8] M. Kim, D. Lee, M. Qi, and J. Kim, "Techno-economic analysis of anion exchange membrane electrolysis process for green hydrogen production under uncertainty," *Energy Conv. Manage.*, vol. 302, p. 118134, 2024.
- [9] C. Lamy and P. Millet, "A critical review on the definitions used to calculate the energy efficiency coefficients of water electrolysis cells working under near ambient temperature conditions," *J. Pow. Sour.*, vol. 447, p. 227350, 2020.
- [10] V. Liso, G. Savoia, S. S. Araya, G. Cinti, and S. K. Kær, "Modelling and experimental analysis of a polymer electrolyte membrane water electrolysis cell at different operating temperatures," *Energies*, vol. 11, no. 12, p. 3273, 2018.
- [11] W. Olbrich, T. Kadyk, U. Sauter, M. Eikerling, and J. Gostick, "Structure and conductivity of ionomer in PEM fuel cell catalyst layers: a model-based analysis," *Sci. Rep.*, vol. 13, no. 1, p. 14127, 2023.
- [12] A. Vorobev, O. Zikanov, and T. Shamim, "A computational model of a PEM fuel cell with finite vapor absorption rate," *J. Pow. Sour.*, vol. 166, no. 1, pp. 92-103, 2007.
- [13] H. Wu, X. Li, and P. Berg, "On the modeling of water transport in polymer electrolyte membrane fuel cells," *Electrochim. Acta*, vol. 54, no. 27, pp. 6913-6927, 2009.
- [14] Y. Zheng, U. Ash, R. P. Pandey, A. G. Ozioko, et al., "Water uptake study of anion exchange membranes," *Macromolecules*, vol. 51, no. 9, pp. 3264-3278, 2018.
- [15] M. L. Disabb-Miller, Z. D. Johnson, and M. A. Hickner, "Ion motion in anion and proton-conducting triblock copolymers," *Macromolecules*, vol. 46, no. 3, pp. 949-956, 2013.
- [16] Y. S. Li, T. S. Zhao, and W. W. Yang, "Measurements of water uptake and transport properties in anion-exchange membranes," *Int. J. Hydrogen Energy*, vol. 35, no. 11, pp. 5656-5665, 2010.
- [17] P. Trinke, B. Bensmann, S. Reichstein, R. Hanke-Rauschenbach, and K. Sundmacher, "Hydrogen permeation in PEM electrolyzer cells operated at asymmetric pressure conditions," *J. Electrochem. Soc.*, vol. 163, no. 11, p. F3164, 2016.
- [18] X. Luo, A. Wright, T. Weissbach, and S. Holdcroft, "Water permeation through anion exchange membranes," *J. Pow. Sour.*, vol. 375, pp. 442-451, 2018.
- [19] S. Fu, J. Song, C. Zhu, G. L. Xu, K. Amine, et al., "Ultrafine and highly disordered Ni₂Fe₁ nanofoams enabled highly efficient oxygen evolution reaction in alkaline electrolyte," *Nano Energy*, vol. 44, pp. 319-326, 2018.
- [20] N. Mahmood, Y. Yao, J. W. Zhang, L. Pan, X. Zhang, et al., "Electrocatalysts for hydrogen evolution in alkaline electrolytes: mechanisms, challenges, and prospective solutions," *Adv. Sci.*, vol. 5, no. 2, p. 1700464, 2018.
- [21] D. Henkensmeier, M. Najibah, C. Harms, J. Žitka, et al., "Overview: State-of-the-art commercial membranes for anion exchange membrane water electrolysis," *J. Electrochem. En. Conv. Stor.*, vol. 18, no. 2, p. 024001, 2021.
- [22] R. J. Gilliam, J. W. Graydon, D. W. Kirk, and S. J. Thorpe, "A review of specific conductivities of potassium hydroxide solutions for various concentrations and temperatures," *Int. J. Hydrogen Energy*, vol. 32, no. 3, pp. 359-364, 2007.
- [23] H. Ito, N. Kawaguchi, S. Someya, T. Munakata, et al., "Experimental investigation of electrolytic solution for anion exchange membrane water electrolysis," *Int. J. Hydrogen Energy*, vol. 43, no. 36, pp. 17030-17039, 2018.
- [24] P. Fortin, T. Khoza, X. Cao, S. Y. Martinsen, A. O. Barnett, et al., "High-performance alkaline water electrolysis using Aemion™ anion exchange membranes," *J. Pow. Sour.*, vol. 451, p. 227814, 2020.
- [25] I. Vincent, A. Kruger, and D. Bessarabov, "Hydrogen production by water electrolysis with an ultrathin anion-exchange membrane (AEM)," *Int. J. Electrochem. Sci.*, vol. 13, no. 12, pp. 11347-11358, 2018.
- [26] I. V. Pushkareva, A. S. Pushkarev, S. A. Grigoriev, P. Modisha, and D. G. Bessarabov, "Comparative study of anion exchange membranes for low-cost water electrolysis," *Int. J. Hydrogen Energy*, vol. 45, no. 49, pp. 26070-26079, 2020.
- [27] V. Schröder, B. Emonts, H. Janßen, and H. P. Schulze, "Explosion limits of hydrogen/oxygen mixtures at initial pressures up to 200 bar," *Chem. Eng. Tech.: Ind. Chemistry- Plant Equip. Proc. Eng. - Biotech.*, vol. 27, no. 8, pp. 847-851, 2004.